Title
SYNTHESIS, BULK AND SURFACE CHARACTERIZATION OF NIOBIUM DOPED Fe2O3. SINGLE CRYSTALS

Author
Sanchez, C.

Publication Date
1985

LBL-19022
Preprint

Lawrence Berkeley Laboratory
UNIVERSITY OF CALIFORNIA

Materials & Molecular Research Division

Submitted to Journal of Solid State Chemistry

SYNTHESIS, BULK AND SURFACE CHARACTERIZATION OF NIOBIUM DOPED Fe_2O_3 SINGLE CRYSTALS

C. Sanchez, M. Hendewerk, K.D. Sieber,
and G.A. Somorjai

January 1985

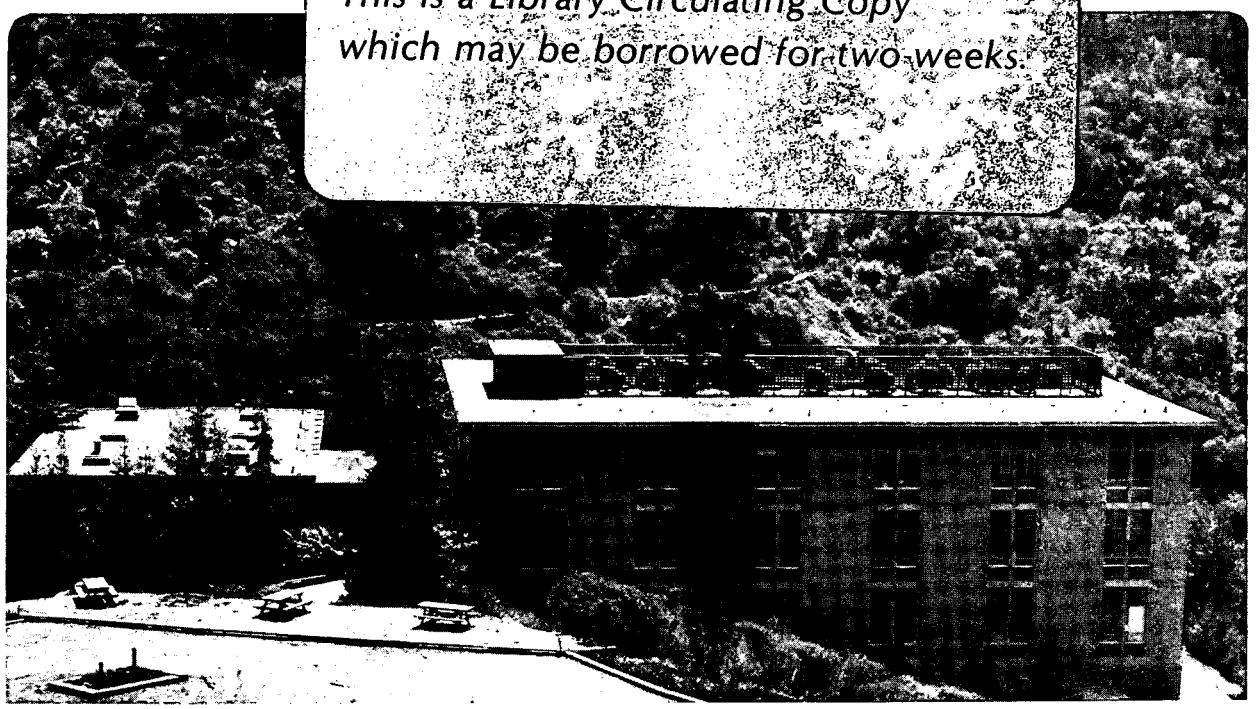

Prepared for the U.S. Department of Energy under Contract DE-AC03-76SF00098

DISCLAIMER

LBL-19022

SYNTHESIS, BULK AND SURFACE CHARACTERIZATION OF NIOBIUM DOPED Fe_2O_3 SINGLE CRYSTALS

C. Sanchez, M. Hendewerk, K.D. Sieber, and G.A Somorjai

Lawrence Berkeley Laboratory
University of California
Berkeley, California 94720

January 1985

SYNTHESIS, BULK AND SURFACE CHARACTERIZATION OF NIOBIUM DOPED Fe_2O_3 SINGLE CRYSTALS

C. Sanchez, M. Hendewerk, K.D. Sieber, G.A. Somorjai

Abstract

Single crystals of niobium substituted α-Fe_2O_3 were grown by using chemical vapor transport with tellurium tetrachloride and were characterized by using bulk methods (x-rays, resistivity, magnetism) and surface techniques (LEED, Auger, XPS). Niobium substituted α-Fe_2O_3 crystallizes with the corundum structure, and is an extrinsic n-type semiconductor with a room temperature resistivity of approximately 85Ωcm, and an activation energy for conductivity of 0.22eV. Low temperature susceptibility measurements suggest that the substitution of niobium(V) in octahedral sites leads to reduction of iron(III) to iron(II) without spinel phase inclusions. The main face of the single crystal platelets is the (001) basal plane of α-Fe_2O_3. The surface is very well ordered as shown by LEED. These crystals show good potential for application in both photoelectrochemistry and surface science studies.

INTRODUCTION

The interesting catalytic and photoelectrochemical properties of iron oxide are linked to its behavior as a semiconductor (1)(2). Stoichiometric hematite, α-Fe_2O_3, is intrinsically an n-type semiconductor with a bandgap of 2.2eV (3)(4) (visible light), but is an insulator at room temperatures ($R>10^6\Omega cm$) (5)(6). Iron oxide is inexpensive, is extremely stable under acidic and basic aqueous conditions, and useful optical properties (good matching between the bandgap and the solar spectrum and a large absorption coefficient).

It is possible to produce a less resistive semiconducting oxide material by reducing some of the iron(III) to the iron(II) state (7). Hematite is then a mixed valence compound with enhanced conductivity at room temperature which are due to a hopping process of electrons between Fe^{2+} and Fe^{3+} ions (6). The Fe^{2+} can be introduced by producing oxygen deficiencies or by adding a dopant which induces a charge compensation process. However, the corundum α-Fe_2O_3 phase has a low solubility for M^{2+} ions since an $Fe(III)_{2-x}Fe(II)_xO_3$ stoichiometry induces the formation of the Fe_3O_4 spinel phase. Thus it is difficult to prepare homogeneous semiconducting samples of Fe_2O_3 in which semiconductive properties do not arise from Fe_3O_4 phase inclusions. It has been shown that it is possible to prepare ternary solid solutions of Fe_2O_3 with TiO_2 (8) and ZrO_2 (9) which are conducting and which do not contain spinel phase inclusions. We have recently synthesized germanium doped Fe_2O_3 single crystals (10) which are also conductive without spinel phase inclusions and which exhibit good photoelectrochemical properties. However, because the germanium ions are smaller than iron ions the germanium can either substitute for iron in an octahedral site in the iron oxide lattice or occupy an interstitial tetrahedral site. Kennedy et. al. have shown that it is possible to dope iron oxide with niobium,

in the form of sintered pellets, which do exhibit photoelectrochemical behavior (2). For this work we have chosen to dope single crystals of Fe_2O_3 with niobium. Because of the extended 4d orbitals niobium will be forced to occupy a substitutional octahedral site.

In this paper we report the preparation and characteristic properties of $Fe_{2-x}Nb_xO_3$ ($x<2\%$) single crystals. We have prepared very high quality crystals by chemical vapor transport have characterized them by bulk methods (x-rays, magnetic susceptibility, electrochemistry) and surface analytical techniques (Auger, XPS, LEED). It was found that Nb substituted Fe_2O_3 crystallizes with the corundum structure and with no spinel phase inclusions. The crystals are large with surface areas of $5mm^2$ to $35mm^2$ and thicknesses of 0.1 to 1mm. Low energy electron diffraction patterns were obtained from these crystals before cleaning or annealing the surfaces, which indicates that the crystal surfaces are very well ordered. They do not have reconstructed surfaces or ordered defects and contain very little carbon or other impurities. Very few studies have been carried out with the $Fe_{2-x}Nb_xO_3$ ternary system, yet we find that these materials are quite active as photoanodes and as materials to study photooxidation processes.

EXPERIMENTAL

Single crystals of niobium substituted Fe_2O_3 were prepared by chemical vapor transport using tellurium(IV) tetrachloride as a transport agent. Approximately 1 gram of charge consisting of Fe_2O_3 (MCB reagent) with 1 mole percent of elemental niobium was placed in a 15cm x 13mm I.D. silica tube along with approximately 20mg of Te metal. The tube was then evacuated to below 1 micron and backfilled with 400 torr of chlorine gas then sealed. An identical procedure was used to prepare pure Fe_2O_3 crystals for comparison, except that the addition of niobium to the charge was omitted. The tubes were

then placed in the zone transport furnace and after 24 hours of back transport from 900°C to 800°C the charge was transported for 10 days. The temperature of the charge zone was 890°C and that of the growth zone 780°C.

After 10 days the furnace was turned off and left to cool to room temperature. The tubes were then removed from the furnace, opened under vacuum, and the product washed with dilute nitric acid, rinsed with water, then dried with acetone. The 6 x 5 x 1 mm platelets shown in Figure 1 were grown using this technique. The major face of the crystals, as determined by x-ray diffraction was the (001) basal plane.

BULK CHARACTERIZATION

X-ray powder diffraction was performed on ground single crystal powders using a Siemens model D500 powder diffractometer equipped with monochromated Cu Kα radiation. Fast scans were carried out using a scan rate of 6° 2θ/min for phase identification. Slow scans for lattice parameter determination were carried out using a scan rate of 0.5° 2θ/min and lattice parameters were calculated using a least squares refinement technique with the aid of a computer. All cell parameters were calculated using hexagonal indexing, and all crystalline directions referred to hereafter are with reference to the hexagonal unit cell.

The electrical properties of samples were measured using the Van der Pauw (11) four probe technique and all crystals were measured in the (001) basal plane. Contacts to the samples were made using an indium-gallium eutectic and the ohmicity of the contact was verified by repetitive measurement of the resistivity at several different current magnitudes between 10μA and 100mA. The variation of the electrical resistivity with temperature was measured using the same techniques except that the ohmic contacts were provided by ultrasonic soldering of pure indium metal. The carrier type of the conducting crystals was determined by qualitative measurement of the Seeback voltage at room temperature.

The magnetic properties of ground single crystal powders were investigated using an S.H.E. Corporation "SQUID" susceptometer. The magnetic susceptibility of samples was measured at varying field strengths between 5 and 25kG in the temperature region between 200K and 10K to examine the field dependence of the sample susceptibility at various temperatures.

SURFACE CHARACTERIZATION

Surface analysis experiments were carried out in an ultra high vacuum chamber with a base pressure of 2×10^{-10} torr. The chamber is equipped with Physical Electronics instruments for low energy electron diffraction (LEED), x-ray photoelectron spectroscopy (XPS), Auger, and argon ion bombardment. The detector used was a double pass cylindrical mirror analyzer. First order diffraction patterns (LEED) were obtained with an incident electron beam energy of 68eV. XPS spectra were obtained using the Kα x-rays from a Mg anode as excitation radiation. The binding energies were measured with respect to the C(1s) peak which was assumed to be 284.5eV. Auger analysis was performed using an incident electron beam of 2 keV energy and 1 mA emission current. The crystals were cleaned using Ar ion bombardment. The argon gas pressure was maintained at 5×10^{-5} torr and the ion gun operated at 1.5 keV and 10mA. Samples were sputtered for very short times in order to remove carbonaceous deposits but not reduce the sample significantly. The crystals were annealed at ~700°C by resistively heating the tantalum foil on which the crystal was mounted.

PHOTOELECTROCHEMICAL MEASUREMENTS

The cyclic voltammetry measurements were carried out using a Pine RDE-3 potentiostat in a standard three electrode configuration with a platinum counter electrode and an SCE reference electrode in an all quartz cell. The illumination source was a 300W tungsten halogen lamp. The light was passed through an IR filter to reduce heating of the sample. The intensity of the focussed light as

determined with a calibrated thermopile was approximately 30mW/cm^2. The electrolyte was 1 molar NaOH prepared using distilled deionized water and Mallenckrodt analytical grade NaOH pellets. Electrodes of niobium substituted Fe_2O_3 were prepared by mounting the crystals on a copper plate with an indium-gallium eutectic to provide an ohmic contact. The copper plate was attached to a glass covered metallic lead, and the entire assembly was insulated with a silicon resin.

RESULTS AND DISCUSSION

X-RAY STUDIES

The results of the crystal growth experiments show that Nb substituted Fe_2O_3 can be grown under the same conditions as pure Fe_2O_3. α-Fe_2O_3 itself crystallized with the corundum structure which can be described as a hexagonal close packed array of oxygen anions in which two thirds of the octahedral interstices are occupied by cations. X-ray powder diffraction patterns of the Nb substituted and pure ground single crystals indicated single phase corundum patterns in all cases. It was concluded that the niobium substituted and pure materials are therefore isostructural. The major face of the single crystals was the (001) basal plane, and the least squares lattice parameters determined for niobium substituted Fe_2O_3 are a = 5.033Å, b = 13.74Å. These results are the same as those of pure Fe_2O_3 (12) and in good agreement with several examples given for single crystals prepared by CVT (10)(13).

In order to determine the composition of the solid solution of niobium in the corundum lattice we have performed elemental analysis of the niobium doped α-Fe_2O_3 crystals using a scanning electron microscope equipped with a Kevex probe. These experiments show the presence of niobium at a concentration of approximately 1.4 atomic percent, which is very near the detection limit of the KEVEX probe. These results suggest that the niobium concentration in our substituted crystals is around two mole percent or less. This is in complete

agreement with the phase diagram for $Fe_{2-x}Nb_xO_3$ ternaries, which indicates an α-Fe_2O_3 solid solution of niobium at low concentration, less than 2 $\pm$ 1% (14). Moreover, ternary systems like $Fe_4Nb_2O_9$ also crystallize with the corundum structure (15), and this probably accounts for the existence of a solid solution of niobium in the α-Fe_2O_3 with conservation of the corundum structure. It is obvious that the apparent lack of change in the lattice parameters of the niobium substituted Fe_2O_3 relative to the pure phase is due to the fact that only a very small amount of niobium was substituted into the lattice.

ELECTRICAL PROPERTIES

The room temperature resistivity of single crystals of $Fe_{2-x}Nb_xO_3$ ($x \sim 0.015$ is about 85 $\pm$ 5Ωcm while that of pure Fe_2O_3 crystals grown under the same conditions is greater than $10^6\Omega$cm. These values are in good agreement with values reported in the literature for Zr and Ti doped Fe_2O_3 (9)(16). The decrease in resistivity is explained by the substitution of iron(III) by niobium (V) in the corundum lattice which leads to a reduction of iron(III) to iron(II).

Qualitative measurements of the Seebeck voltage showed the Nb substituted Fe_2O_3 to be an n-type semiconductor. Quantitative Seebeck experiments and electrical measurements carried out on doped Fe_2O_3 (5)(6) have shown that the mobility in these materials is thermally activated (5)(6)(7)(17) and that conductivity occurs via an electronic hopping between Fe(II) and Fe(III).

A plot of the logarithm of resistivity versus 1/T for niobium doped Fe_2O_3 is shown in Figure 2. In the range of temperature (160K to 300K) this curve follows an Arrhenius behavior. From the slope of this curve we can extract the activation energy of the conductivity which is about 0.22eV. This value is consistent with those reported in the literature for materials based on iron oxide (7)(10). Small differences between the activation energy for germanium doped Fe_2O_3, 0.12, (7) and niobium doped Fe_2O_3, can be accounted for from a

small shift in the Fermi level which occurs as a result of the differences in the carrier concentrations of these two crystals. Assuming a mobility at room temperature of about 0.1cm^2Vs (17) for these materials, and taking their respective values of the restivity (R = 5Ωcm for germanium doped α-Fe_2O_3, and R = 85Ωcm for niobium doped α-Fe_2O_3), this gives rise to the following carrier densities: $N_D(Fe_{2-x}Ge_xO_3) = 1.25 \times 10^{19}cm^{-3}$ and $N_D(Fe_{2-x}Nb_xO_3) = 7.4 \times 10^{17}cm^{-3}$. A lowering of the Fermi level of about 0.06eV is expected for each order of magnitude decrease in donor densities (18), which is consistent with the difference of about 0.1eV between our Nb and Ge doped crystals.

MAGNETIC SUSCEPTIBILITY

Although the x-ray diffraction patterns of the powdered single crystals indicate that the corundum structure is the only phase present, the possibility still exists that Fe_3O_4 phase inclusions below the detection limit of x-ray diffraction might be present. Fe_3O_4 inclusions in the Fe_2O_3 lattice can also produce an n-type semiconductor (19). The electrical conduction in that case would occur through a percolation of carriers provided by the spinel phase inclusions because Fe_2O_3 is a high resistivity material while Fe_3O_4 is a semimetal at room temperature (7). The presence of Fe_3O_4 phase inclusions in Fe_2O_3 can be detected by measuring the magnetic susceptibility of the material at various magnetic field strengths. If Fe_3O_4 phase inclusions were present in these materials a constant and dramatic field dependence on temperature should be observed. There would be no contribution to the magnetic field dependence from Fe_2O_3 because hematite is antiferromagnetically ordered in the temperature domain (10K - 200K) studied.

A Honda Owens plot representing the variation of magnetic susceptibility with reciprocal field strength for Nb substituted Fe_2O_3 is presented in Figure 3. The plot for Fe_2O_3 is shown in the same Figure. The temperature range

investigated is 10K to 200K, well below the Curie Temperature of Fe_3O_4. The Honda Owens plot should exhibit a distinct positive slope if ferrimagnetic Fe_3O_4 inclusions are present in our materials. Two important observations can be made from these experiments. The first is that the magnitude of the magnetic susceptibility is the same in the Nb substituted Fe_2O_3 as in the pure Fe_2O_3. The second is that our Honda Owens plots exhibit slightly negative slopes, indicating a weakly antiferromagnetic coupling. From these observations we can conclude that the Nb doped Fe_2O_3 single crystals are free of spinel phase inclusions and are homogeneous materials.

The magnetic properties of the Nb substituted Fe_2O_3 are slightly different from those which we recently reported for Ge substituted Fe_2O_3 (10). In the latter case the Honda Owens plot exhibited almost constant but slightly positive slopes. This difference in magnetic properties may be due to differences in the substitutional nature of the Ge and Nb atoms in the corundum lattice. It is more probable that niobium is really replacing an iron(III) atom in an octahedral site rather than occupying an intersitial tetrahedral site because Nb is a large ion with extensive 4d orbitals. This is supported by the experiment reported by Bertaut. He found, by using magnetic measurements and neutron diffraction, that niobium occupies the octahedral site in corundum structures like $Fe_4Nb_2O_9$ (15). Germanium, on the other hand, is smaller than the Fe and would be expected to substitute in intersitial sites satisfying the tendency of smaller cations to favor tetrahedral coordination. It might be useful to perform experiments such as ESR to characterize the paramagnetic defects of doped iron oxides in order to elucidate the exact role of the dopant in these materials.

SURFACE CHARACTERIZATION

In addition to the high purity and homogeneity of the Nb doped crystals in the bulk, we have found that the crystal surfaces are also homogeneous and

virtually free of defects or impurities directly after the preparation procedure. The major face of the crystals was determined to be the (001) basal plane by bulk x-ray diffraction. A pictorial representation of this hexagonal packed array of oxygen atoms with octahedrally coordinated iron atoms is shown in Figure 4. A LEED pattern of the Nb doped single crystals is also shown in Figure 4. The hexagonal pattern is indicative of the (001) face as can be seen by the cross sectional representation. This LEED pattern was obtained from the crystals, as received. The intensity of the diffraction spots was low but easily detectable. Auger analysis of the crystals showed that several monolayers of carbon are present on the freshly prepared surfaces which attenuates the intensity of the iron oxide crystal diffraction spots. After cleaning the sample with argon ion bombardment for several minutes and subsequently annealing the crystal to ~700°C for 10 minutes, no trace of carbon was seen by Auger. The LEED pattern became very sharp but did not change, indicating that the surface was not reconstructed nor had any ordered defects directly after preparation.

The Auger analysis of the samples before the argon ion bombardment showed the presence of oxygen, iron, niobium, carbon, and trace amounts of chlorine (from the charge in the transport). After cleaning the crystal, no impurities were detected. XPS spectra were used to quantitatively measure the relative amounts of iron, oxygen, and niobium. These results showed that Nb was present at the surface in amounts of <1%, while the Auger peak to peak ratio of O(510)/Fe(651) was 3.0 $\pm$ 0.2 in agreement with previous Auger studies (20).

DC VOLTAMMETRY EXPERIMENTS

DC voltammetry experiments were carried out as a simple test of the photoelectrochemical properties of the Nb doped single crystals. They were performed on the (001) basal plane of the crystals in one molar NaOH solution. The cyclic voltammograms observed under cathodic and anodic bias exhibited the characteris-

tics of an ideal n-type semiconductor diode. The voltammograms measured in the dark showed very low dark currents, well below $1\mu A/cm^2$ in the range between -1 V and +0.7 V (SCE). DC voltammograms taken from crystals under the illumination of a tungsten halogen lamp showed photocurrents on the order of 500 to $700\mu A/cm^2$ at +0.4 V (SCE) as shown in Figure 5. These photocurrents are most likely due to photoinduced electrolysis of water. Continuous cycling experiments showed that these materials were stable under illumination. There was no observable attenuation of the photocurrents and no visible tarnishing of the crystal surface.

The qualitative behavior of the single crystal electrodes is in good agreement with that of α-Fe_2O_3 photoanode materials reported in the literature (2) (10)(21)(22), except that no photocathodic currents were ever observed at negative potentials (22)(19). There is an additional interesting feature which is observable in the cyclic voltammograms of these Nb doped Fe_2O_3 crystals. These crystals exhibit a second photooxidation process which is depicted in Figure 5 as wave A. When cycling the electrode from -1.0 V to 0.7 V (SCE) with the light on, the photooxidation wave A appears. If the light is switched off as the cycling continues from +0.7 V to -1.0 V, wave B appears - even under these dark conditions. If we start at the positive potential with the light on, before the potential at which wave B should appear, we do not obtain the reduction wave. But if we turn the light on as we continue the cycle, sweeping anodically, wave A appears. The redox potential at which this oxidation reduction process occurs is approximately -0.2 V (SCE) in a solution of pH = 14. This value shifts by about 25 mV per pH unit which implies that the redox reaction is a two electron process. After etching the crystal in H_2O_2 or after a few days of electrochemical experiments this phenomenon disappears.

In summary, the reduction wave occurs both in the light and the dark, but

only after cycling through the oxidation region. This implies that either the oxidation is reversible or that a species on the surface is being oxidized to form a species which is then reduced to a non-reactive form which remains on the surface or is desorbed. The fact that the phenomenon disappears with time or with H_2O_2 etching makes the latter presumption most plausible.

Despite the behavior of this unknown redox reaction the quantum efficiency for the photodissociation of water for these materials does not change with time The quantum efficiency is around 40% for these Nb doped crystals at a bias of +0.5 V (SCE) with 370nm illumination both before and after the waves at -0.2 V vs SCE are gone, which is more than twice that reported for most doped iron oxide materials (23)(24). A more quantitative photoelectrochemical study is in progress (25).

CONCLUSIONS

It has been shown that a homogeneous conducting corundum phase of Fe_2O_3 can be prepared by chemical vapor transport from the ternary solution of $Fe_{2-x}Nb_xO_3$ where $0 < x < 0.02$. Niobium substituted Fe_2O_3 crystallizes with the corundum structure and is an n-type semiconductor which behaves well as an electrochemical anode for the photooxidation of water. The room temperature resistivity of 85Ωcm for these crystals is significant since one of the barriers toward using iron oxide more successfully as a photoanode has been the high intrinsic resistivity of the undoped material. Magnetic susceptibility studies suggest that the conductivity of the samples arises from charge compensation resulting from reduction of iron(III) to iron(II) upon niobium substitution in the structure. Electrical measurements give an activation energy for the electron hopping of 0.22eV.

The surfaces of these crystals have also been shown to be of the same composition as the bulk which emphasizes the homogeneity of the material. Composition-

al analysis by Auger electron spectroscopy indicates that there is a layer of carbon on the surface which is easily removed by argon ion bombardment. Most important is the fact that we can obtain a LEED pattern from these single crystals directly after preparation. The hexagonal LEED pattern observed agrees with the bulk x-ray diffraction data showing that the crystals have grown in the orientation of the (001) face of the corundum structure. XPS data show that the concentration of Nb at the surface is on the same order as that in the bulk, i.e. that there is no surface segregation of the Nb. The O/Fe ratio from XPS is also indicative of the Fe_2O_3 phase.

The large size of these crystals combined with the homogeneity of the surface and bulk make these materials a good prototype for studying catalytic or simulated electrochemical reactions in an ultra high vacuum chamber. The photoanode behavior of the Nb doped crystals competes well both qualitatively and quantitatively with doped polycrystalline samples. Because these crystals are very homogeneous, while sintered polycrystalline materials are usually not, these single crystals can be used to understand the fundamental processes (mechanisms) for a variety of reactions.

ACKNOWLEDGEMENTS

This work was supported by the Director, Office of Energy Research, Office of Basic Energy Sciences, Chemical Sciences Division of the U.S. Department of Energy under Contract No. DE-AC03-76SF00098. C.S. would like to acknowledge support from the National Science Foundation under grant number INT/8412371. The authors gratefully acknowledge the cooperation of Dr. R. Kershaw from A. Wold laboratories at the Brown University Materials Research Department for performing the measurements of electrical resistivity versus temperature, and Dr. N. Edelstein and G. Shalinoff for their assistance with the magnetic measurements on the "SQUID" susceptometer in the Materials and Molecular Research Division of Lawrence Berkeley Laboratory.

REFERENCES

1. D. Cornack, R.F. Gardner, R.L. Moss, J. Cat. 17, 219,230 (1970).

2. R. Shinar, J.H. Kennedy, Sol. En. Mat. 6, 323 (1982).

3. W.H. Strehlow, E.L. Cook, J. Phys. Chem., 2, 163 (1973).

4. F.P. Koffyberg, K. Dwight, A. Wold, Sol. St. Comm., 30, 1735 (1979).

5. R.F. Gardner, F. Sweet, D.W. Tanner, J. Phys. Chem. Sol., 24, 1183 (1963).

6. B.M. Warnes, F.F. Aplan, G. Simkovich, Sol. St. Ionics, 12, 271 (1984).

7. J.B. Goodenough, "Metallic Oxides", in Progress in Solid State Chemistry, 5, 145, H. Reiss, Ed. Pergamon Press, N.Y. (1971).

8. J.H. Kennedy, K.W. Freese Jr., J. Elect. Soc., 125(5), 723 (1978).

9. G. Horowitz, J. Electroanal. Chem., 159, 421 (1983).

10. K.D. Sieber, C. Sanchez, J.E. Turner, G.A. Somorjai, J. Chem. Soc. Faraday Trans. I, in press.

11. L.J. Van der Pauw, Phillips Res. Resp., 13, 9 (1958).

12. P. Merchant, R. Collins, K. Dwight, A. Wold, J. Sol. St. Chem., 27, 307 (1979).

13. V. Agafonov, D. Michel, M. Perez y Jorba, M. Fedoroff, Mat. Res. Bull., 19, 233 (1984).

14. A.C. Turnock, J. Am. Ceram. Soc., 49(4), 177 (1966).

15. E.F. Bertaut, L. Corliss, F. Forrat, R. Aleonard, R. Pauthenet, J. Phys. Chem. Sol., 21, 234 (1961).

16. G.H. Geiger, J.B. Wagner, Jr., Trans. Metallurgical Soc. AIME, 233, 792 (1965).

17. H.J. Vandaal, A.J. Bosman, Phys. Rev. 158, 736 (1961).

18. J.F. Dewald, Bell, Sept. Techn. J., 39, 615 (1960).

19. K.D. Sieber, C. Sanchez, J.E. Turner, G.A. Somorjai, Mat. Res. Bull., submitted.

20. M. Seo, J.B. Lumsden, R.W. Staehle, Surf. Sci., 50, 541 (1975).

21. K.L. Hardee, A.J. Bard, J. Elect. Soc., 124, 215 (1977).

22. C. Leygraf, M. Hendewerk, G.A. Somorjai, J. Cat., 78, 314 (1982).

23. R.K. Quinn, R.D. Nasby, R.J. Baughman, Mat. Res. Bull, 11, 1011 (1976).

24. J. Chem. Soc. Faraday Trans. I, 79, 2027 (1983).

FIGURE CAPTIONS

Figure 1. Photograph of Nb-doped iron oxide single crystal platelets 6 mm x 5 mm x 1 mm.

Figure 2. Arrhenius plot of resistance as a function of temperature (log R vs. 1/T) for Nb-doped iron oxide single crystals.

Figure 3. Magnetic susceptibility vs. 1/H for Nb-doped iron oxide single crystals.

Figure 4. A) Model of the corundum (001) structure. The solid circles represent Fe^{3+} ions. The open circles are the first layer of O^{2-} ions, the shaded circles are the second layer of O^{2-} ions. B) LEED pattern of the Nb-doped iron oxide single crystals. Beam energy of 102 eV.

Figure 5. DC voltammogram for Nb-doped iron oxide single crystals.

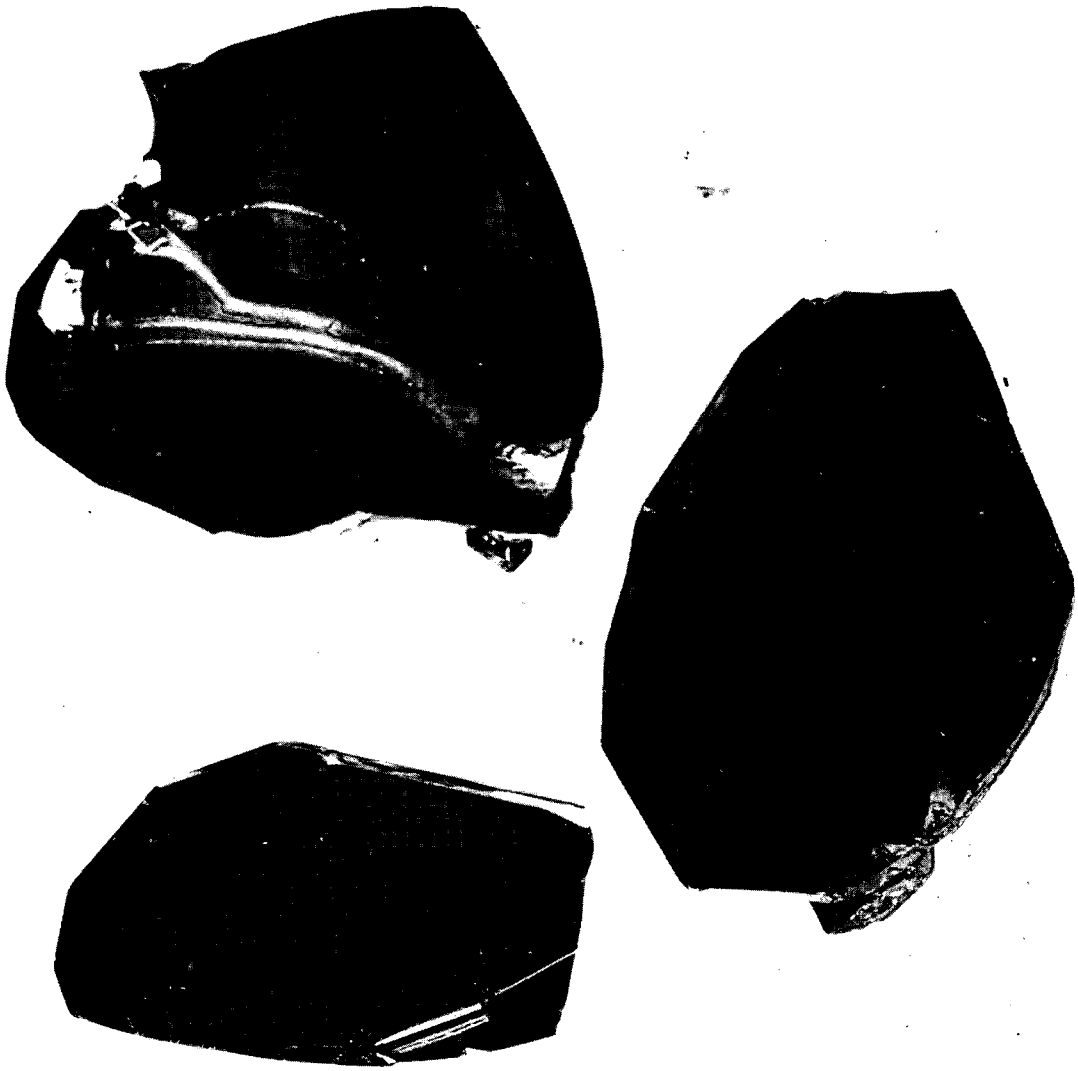

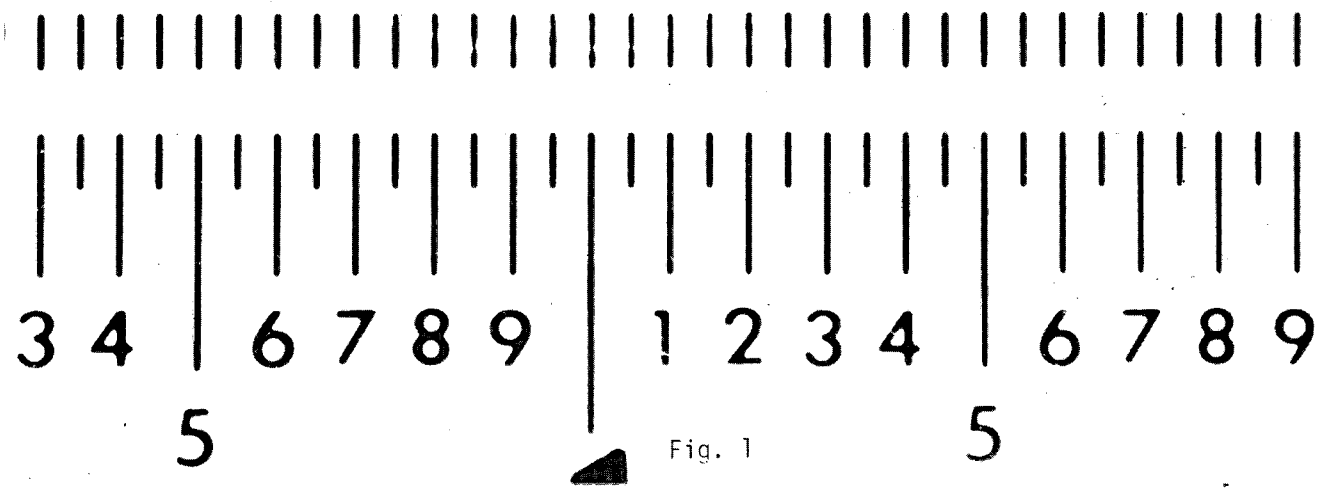

Fig. 1

CBB 849-7825

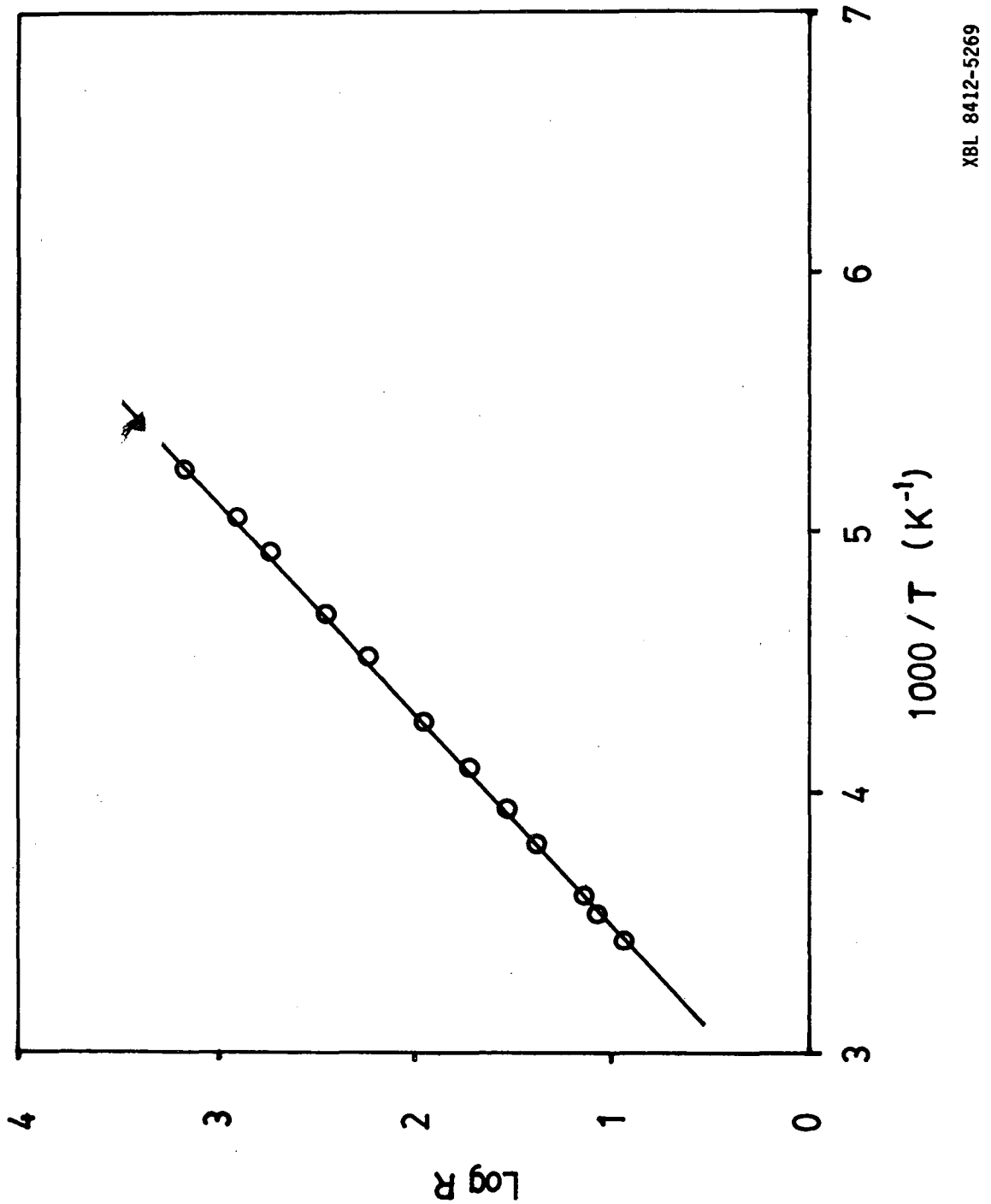

Fig. 2

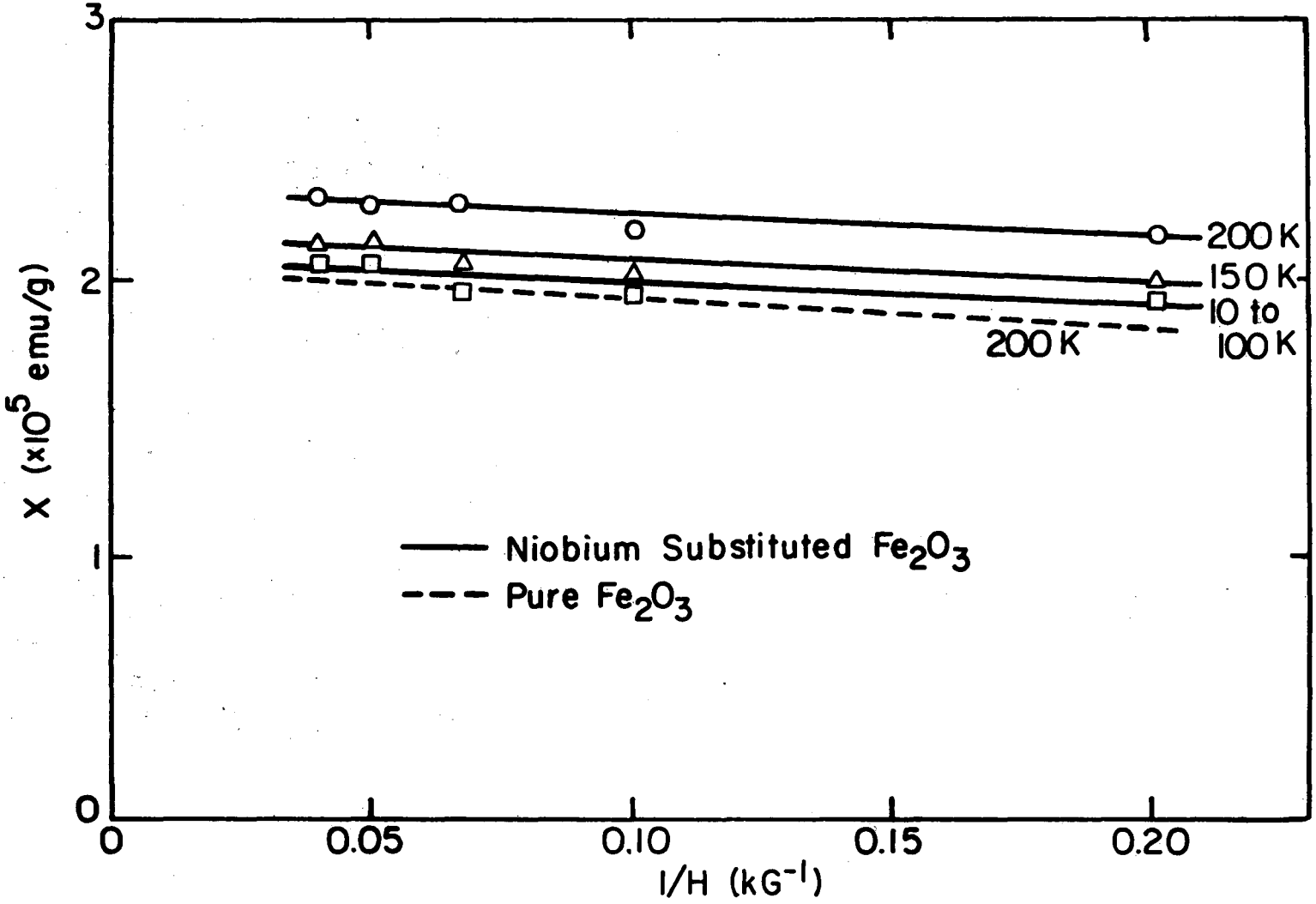
3
2
1
0
0
0.05
0.10
0.15
0.20
X (x10^5 emu/g)
I/H (kG^-1)
200 K
150 K
10 to 100 K
200 K
Niobium Substituted Fe2O3
Pure Fe2O3
XBL 8412-5312

Fig. 3

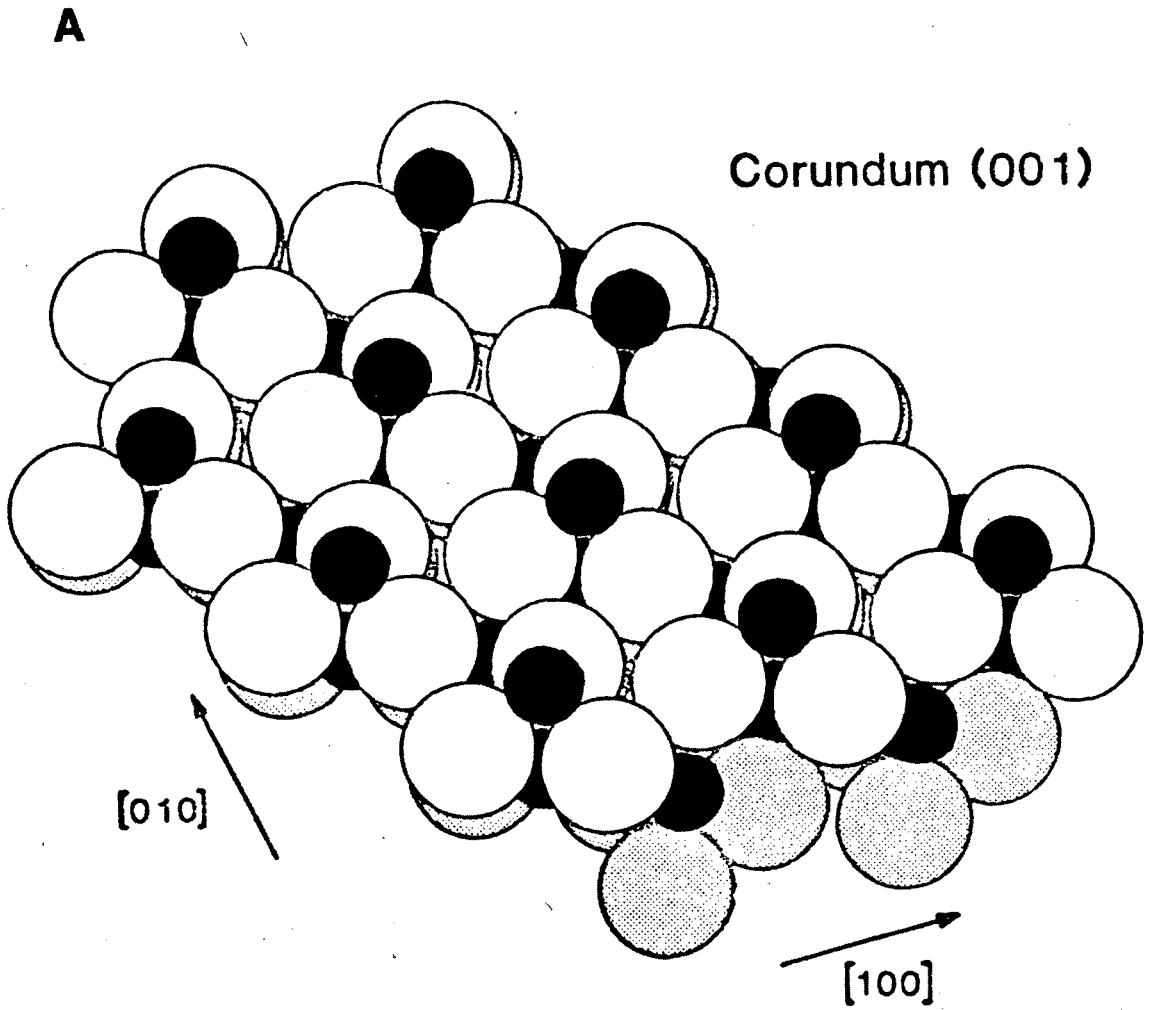

Fig. 4 XBB 840-9098

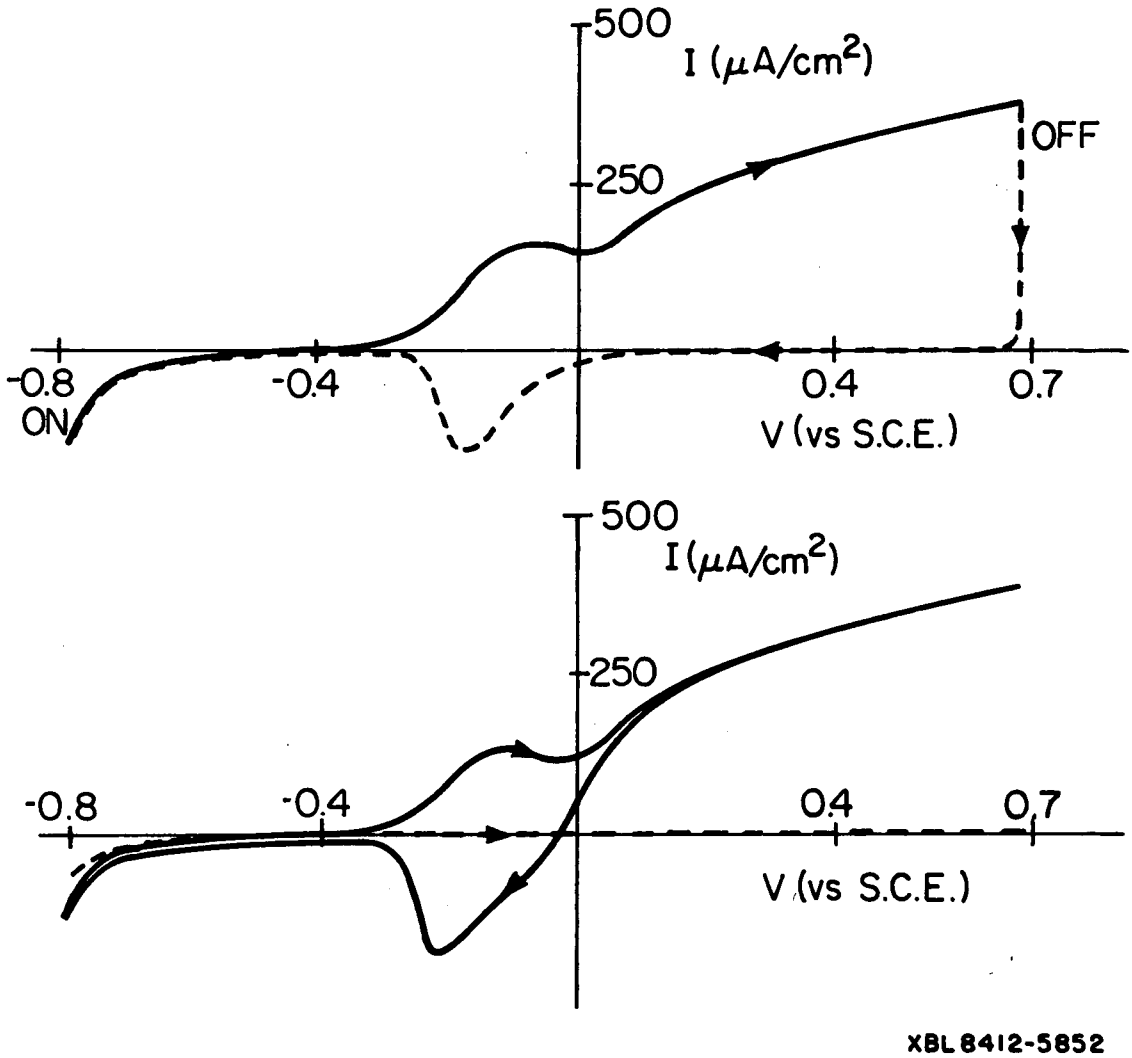
500
I (μA/cm²)
OFF
250
-0.8
ON
-0.4
0.4
0.7
V (vs S.C.E.)
500
I (μA/cm²)
250
-0.8
-0.4
0.4
0.7
V (vs S.C.E.)
XBL 8412-5852

Fig. 5

This report was done with support from the Department of Energy. Any conclusions or opinions expressed in this report represent solely those of the author(s) and not necessarily those of The Regents of the University of California, the Lawrence Berkeley Laboratory or the Department of Energy.

Reference to a company or product name does not imply approval or recommendation of the product by the University of California or the U.S. Department of Energy to the exclusion of others that may be suitable.

TECHNICAL INFORMATION DEPARTMENT
LAWRENCE BERKELEY LABORATORY
UNIVERSITY OF CALIFORNIA
BERKELEY, CALIFORNIA 94720